

Supplementary Methods and Materials:

1.1 Spp virus generation

Spp virus was generated in Phoenix cells after being co-transfected by pLV-mCherry and pcDNA-Spike using a calcium phosphate kit (ThermoFisher, Waltham, MA, USA), which was previously reported [1]. The supernatant containing Spp virus was harvested 48 to 72-hours post transfection, clarified by centrifuging at 5,000 g for 15 min, followed by passing through 0.45 µm filter disk, and precipitated by ultracentrifuging at 24,000 rpm for 2 hours. The viral pellets were resuspended in cold PBS buffer, aliquoted, and stored at -80 °C before use. The viral particle number was determined using real time RT-PCR assay. Co-transfection of pLV-mCherry and pMD2.G vector carrying vesicular stomatitis virus glycoprotein (VSV-G) expression cassette were performed to obtain VSV-G lentivirus [1].

1.2 Real time RT-PCR, Western blot, and Immunostaining

RNA extraction kit was obtained from Zymo Research (Irvine, CA, USA) and Qiagen (Hilden, Germany). The RT kit was obtained from Takara Bio USA (Mountain view, CA, USA). The SYBR green master mix was from Biorad (Hercules, CA, USA). For cDNA synthesis, RT reaction was carried out at 42°C for 2 hrs containing 1x RT buffer, 1.0~5 µg of total RNA, 0.5 mM dNTPs, 0.5 µg of oligo (dT) 15-mer primer, 20 units of RNasin, and 5 units of SMART Moloney murine leukemia virus reverse transcriptase. A combined index of three house-keeping genes beta-actin, Rps18 and Nono were used as controls to normalize the amplification data in real time PCR. The real time PCRs were performed as we previously reported [1]. For Western Blot assay, cellular proteins were extracted from hearts and other organs using RIPA lysis buffer (Santa Cruz Biotech., Inc., Dallas, TX, USA), separated by SDS-PAGE, followed by a transfer onto PVDF membranes. Primary antibodies were added and followed by HRP-labeled secondary antibodies. Images were acquired using a Bio-Rad Gel Imaging System (Hercules, CA, USA). GAPDH, beta-actin, and beta-tubulin were used as internal controls.

For immunostaining, hearts from mice were under snap freezing process and approximately 6 µm thick fresh sections were cut and collected. The sections were then fixed by 10% buffered formalin (Fisher Scientific, Pittsburgh, PA, USA), blocked with 5% donkey serum, and incubated in a humidified chamber overnight at 4°C with primary antibodies, followed by fluorescent conjugated secondary antibodies for 2 hours at room temperature. Images were acquired using ImageXpress Pico System (Molecular Device, San Jose, CA, USA) or confocal microscopy system (Carl Zeiss AG, Oberkochen, Germany).

1.3 Cardiac fibrosis staining

The fibrosis in mouse hearts was evaluated using Masson's trichrome staining (#HT15-1KT, Millipore Sigma). Briefly, the heart cross sections were fixed by Formalin and stained in Weigert's iron hematoxylin working solution, followed by Biebrich scarlet-acid fuchsin solution, phosphomolybdic-phosphotungstic acid solution, and Acetic acid. The sections were dehydrated and mounted. The images were acquired using ImageXpress Pico System (Molecular Device, San Jose, CA, USA). Images from 5-8 sections (60x objective) per heart were analyzed using ImageJ software plug in Color deconvolution 2 and the percentage of fibrotic areas per section

was estimated (n=3 hearts per group). Mann-Whitney test was used to compare the difference among two groups.

Supplementary Discussions:

Statins can upregulate the expression of SR-B1 [2], but such an effect seems unlikely to increase risk of SARS-CoV-2 infection since viral entry can be mitigated by lowering cholesterol levels and altering membrane lipid rafts by statins. Indeed, the use of statins does not alter the SARS-CoV-2 infection in patients [3]. Furthermore, many retrospective observational studies have shown that statin therapy can reduce the risk of severity and mortality and improve prognosis in hospitalized patients with COVID-19 [4, 5]. Mechanistically, statins can attenuate SARS-CoV-2 replication *via* main protease and RNA-dependent RNA polymerase, reduce inflammation, improve endothelial function, decrease risk of thrombosis, and alleviate pulmonary fibrosis in patients with COVID-19 [6, 7]. However, the statin-related side effects such as increase in risk of diabetes may worsen the outcome in inpatients with type 2 diabetes, e.g., elevating COVID-19 related mortality [8].

Pathophysiological mechanisms perpetuating CVD sequelae of PASC are yet to be determined. Both acute and chronic cardiac injuries secondary to SARS-CoV-2 infection are thought to be involved [9]. SARS-CoV-2 virus has been detected in the heart tissue in autopsy studies [10]. Acute infection of SARS-CoV-2 can cause microvascular and myocardial injuries, including endothelialitis, microthrombi, and altered renin-angiotensin homeostasis [11, 12]. In an animal model, SARS-CoV-2 infection results in cardiac pericyte loss, fibrosis, cardiomyocyte hypertrophy, and diastolic dysfunction in hamster [13]. The Spike protein alone can damage cardiac pericytes function [14]. In this study, long-term transcriptomic suppression of mitochondria related respiratory genes are revealed after a transient (one time) exposure of the replication-incompetent Spp virus which viral particles are cleared in 3~4 days after administration in obese mice. This data suggests that potential mitochondria malfunction, probably caused by obese-induced inflammatory responses and subsequently exacerbated by viral infections, is a contributor to the long-term cardiac sequelae in COVID-19 patients. The transition from acute cardiac illnesses to chronic phase in PASC may be possibly explained by several putative mechanisms. First is the chronic inflammatory response evoked by SARS-CoV-2 infection or integration of the SARS-CoV-2 genome into host DNA, which can induce a continuous activation of immune-inflammatory cascades and results in persistent endothelial dysfunction and cardiomyopathy [15]. Second, autoimmune antibodies against cardiac antigens are elicited through molecular mimicry in COVID-19, which may contribute to the delayed damages [16].

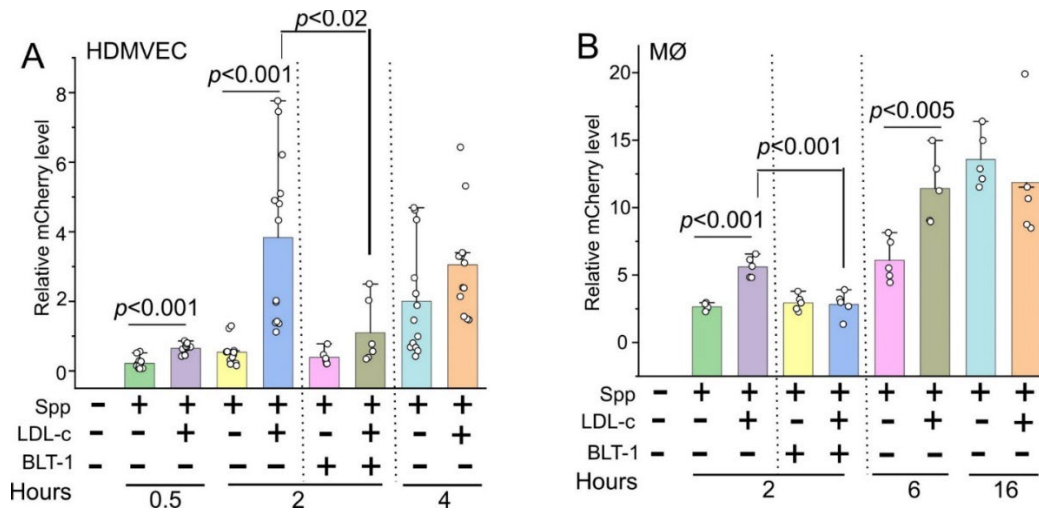
It has been well established that obesity with impaired storage of fat in adipose tissue forces non-adipose tissues, such as the heart, to keep the excess fat, a phenomenon referred to as ectopic fat deposition, which is usually toxic to the non-adipose tissue, i.e. lipotoxicity, leading to obesity-related complications, such as vasculopathy and cardiomyopathy [17, 18]. It is reasonable to posit that SARS-CoV-2 infection interplays thus exacerbates obesity-related cardiac comorbidities. In this study, we have identified upregulations of clusters of genes involving stress signaling, glucose metabolism, and cardiovascular functions. (1) NFE2L1 is a master transcription factor that regulate expression of all the proteasome subunit genes during stress response [19].

Other upregulated DEs with functional characteristics of inflammatory and kinase activity included GBAS, MFN2, GNA12, PI4KB, PIP4K2B, C3, and GIT1. For example, GBAS is localized to mitochondria and plays a role in oxidative phosphorylation and vesicular transport; it can facilitate NF- κ B-mediated cytokine production [20]. *MFN2* is a GTPase embedded in the outer membrane of the mitochondria, involving mitochondria fusion and mitophagy [21]. (2) Genes involve in glucose metabolisms, such as *OGDH*, *OGDHL*, *PYGB*, and *GYS1*. *OGDHL* is a rate-limiting enzyme in the Krebs cycle that is pivotal in mitochondrial metabolism [22]. *PYGB* regulates glycogen mobilization [23]. Under normal conditions, main source of cardiac ATP is from fatty acid oxidation (FAO), but less from glucose metabolism. With mitochondria dysfunction or metabolic perturbations, cardiac metabolic profiles are impaired by reduction in FAO and concomitant increases in glucose utilization [24, 25]. (3) Gene clusters engage in cardiovascular functions. *SCN5A* is a tetrodotoxin-resistant voltage-gated sodium channel subunit and primarily expressed in cardiac muscle for the action potential initiation in an electrocardiogram [26]. *SLC6A6* is a sodium and chloride ion-dependent taurine neurotransmitter transporter, which deficiency leads to cardiomyopathy [27]. *SCARA5* has a function in scavenger receptor activity and ferritin receptor activity, which genetic locus is associated with the susceptibility to venous thromboembolism [28]. *PER1* is a member of the Period family of genes for circadian rhythms, which can regulate cardiovascular rhythm centrally (through brain) and peripherally (in the heart) [29-31]. The upregulation of *PER1* is probably due to the long-term stress or chronic inflammatory consequence in HDF mice after viral administration. *PCSK6* is upregulated in human atherosclerotic plaques associated with smooth muscle cells (SMCs); it induces SMC migration and modulates vascular remodeling [32]. These data demonstrate that long-term chronic inflammations persist in HFD mice after viral administration, leading to cardiac metabolic and functional perturbations.

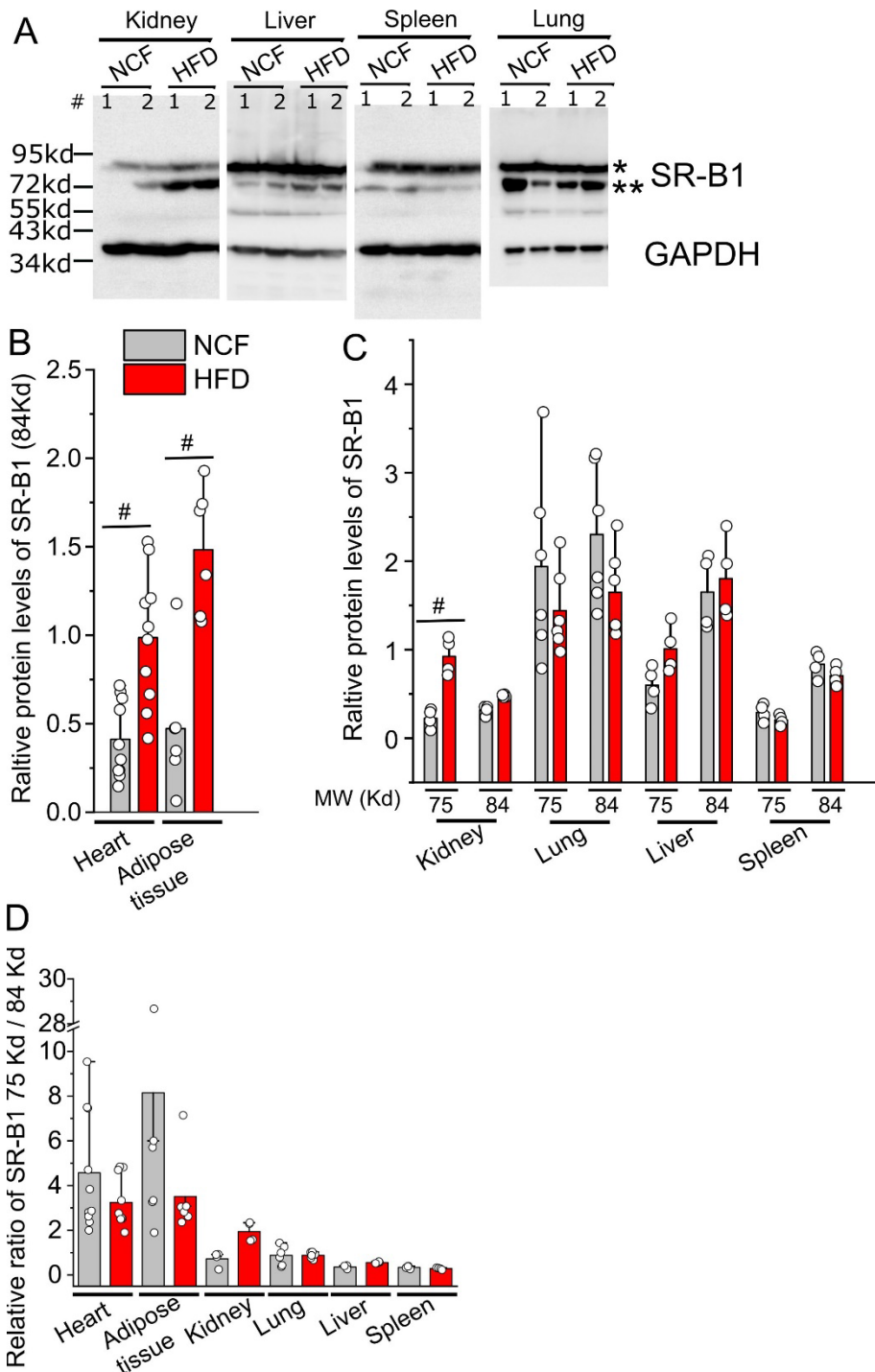
The Spp virus is a replication-incompetent virus. The dosage administered in this study is supraphysiological. The viral burdens were detected in the heart, the liver, kidneys, spleen (around 29~35 Ct values in a real time RT-PCR assay) and lungs (26~30 Ct values) at 2 hpi. At 24 hpi, the Spp virus was hardly detectable in these tissues (33~36 Ct values or negative). Therefore, the viral particles were rapidly and effectively removed from the body. The residual viral burdens retained in the tissues at 2 hpi were in the pathological ranges from the nasal and pharyngeal swab samples in patients (overall median (interquartile range) Ct value: 28.7 (23.9–33.4)) [33]. Our data reflects parts of pathological spectra of PASC. Firstly, exposure of replication-incompetent Spp virus is transient and one time. The viral particles are rapidly cleared and undetectable 3~4 dpi in mice, which can be equivalent to the “viral-free” stage in discharged COVID-19 patients. The timelines from 6 to 24 wpi in this animal model is long enough to mimic potential cardiac sequelae in PASC in patients. Secondly, obesity is associated with and contributes to PASC [34-36]. Our data has demonstrated that cholesterol facilitates viral uptake in host cells and heart is the vulnerable organ for viral accumulation under obesity. Lastly and more importantly, the cardiac functional impairments and fibrotic development have been revealed as long-term sequelae in this model.

The first case series about persistent symptoms after acute COVID-19 was reported in July 2020 in an Italian hospitalized cohort [37], which was posited to be caused by the Wuhan original strain before the Alpha variant emerged to be the dominant variant in the world until January 2021 [38]. Different variants of SARS-CoV-2 may

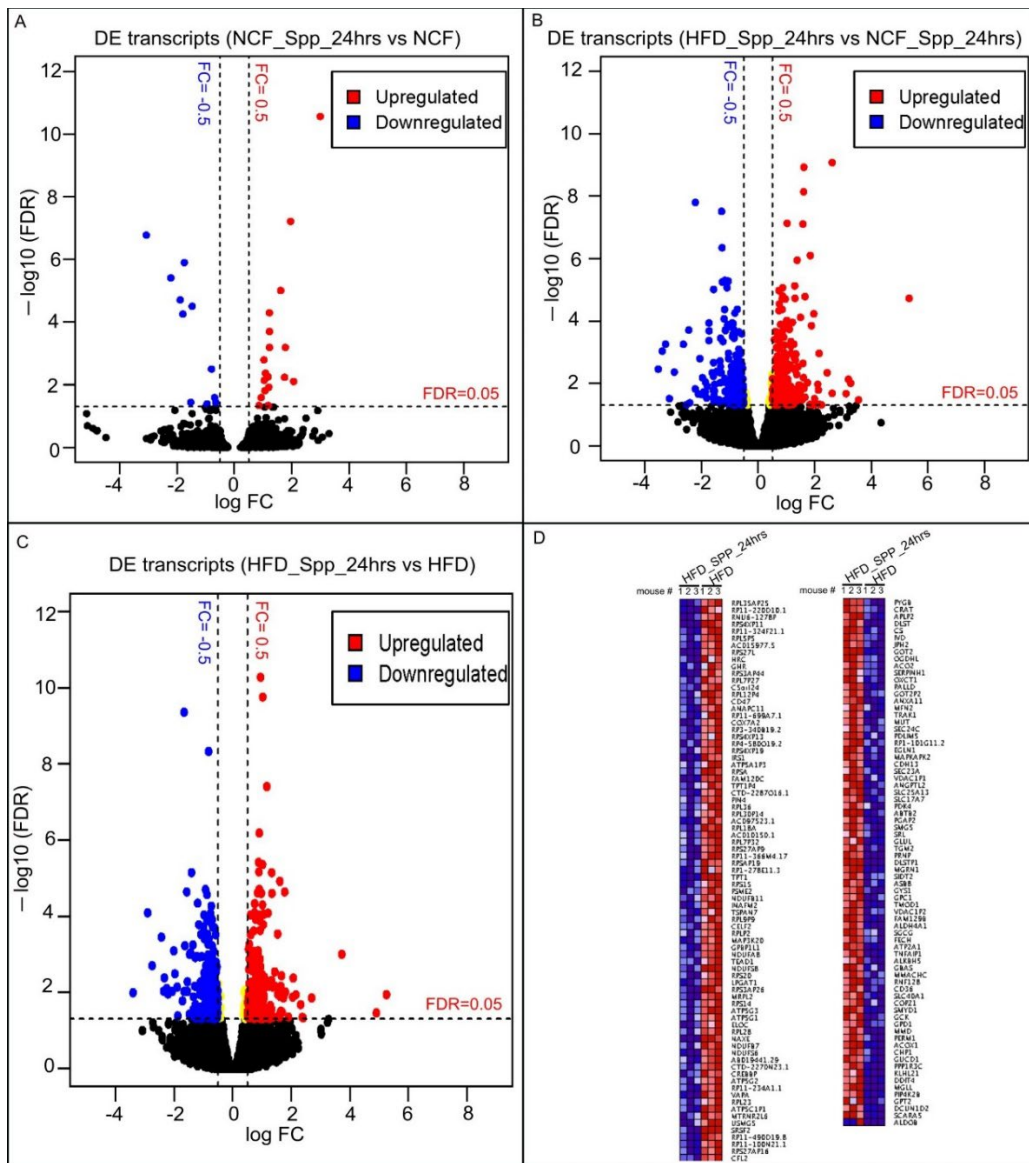
lead to different clinical aspects of PASC. For example, patients infected by the Wuhan variant showed higher incidences of dyspnea than those infected with Alpha or Delta variant [39]. Another report shows that Wuhan variant causes higher occurrences of dysgeusia and anosmia as compared to the Alpha variant in patients [40]. Patients infected by the Omicron variant were less likely to experience PASC than those infected by the delta variant with an odds ratio ranging from 0.24 (0.20–0.32) to 0.50 (0.43–0.59) [41]. It could be expected that PASC from individuals infected with the Wuhan variant would lead to higher burden and health costs than those infected by other variants [39]. The underlying explanations could be as follows. First, the Darwinian evolution of the mutations of Spike protein has led to less pathogenicity but higher transmissibility among VOCs [42, 43]. The Wuhan variant exhibited the highest pathogenicity which led to higher fatalities and likely PASC as well. Second, administration of antiviral medications, e.g., remdesivir, can reduce the risk of PASC [44]. Third, vaccination can reduce PASC [45]. These selective pressures reflected and contributed to the viral evolution and its adaption to a new host.



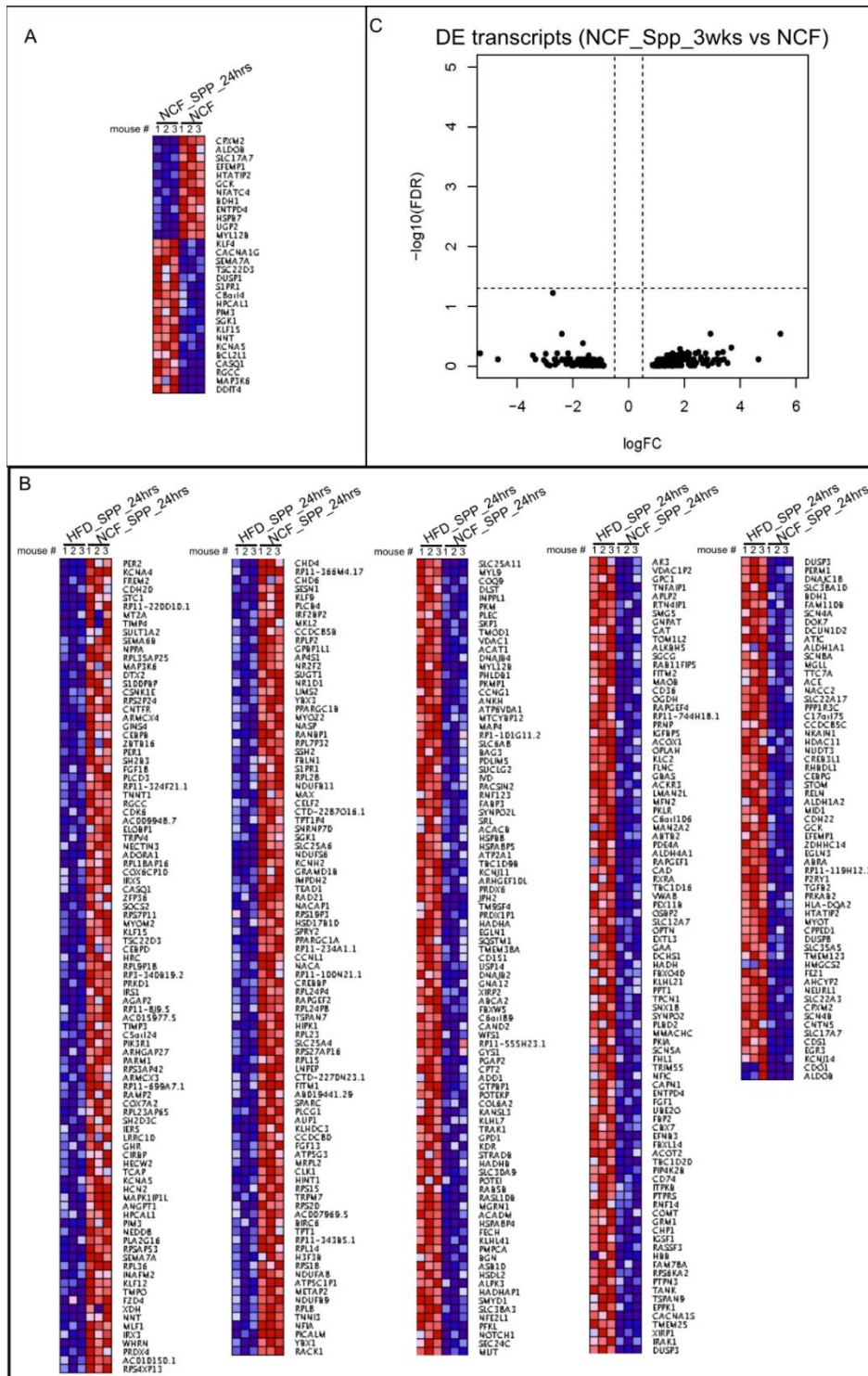
Supplementary Fig 1 LDL-c significantly increases cellular uptake of Spp virus in HDMVEC (A) at 0.5 and 2 hpi and in MØ (B) at 2 and 6 hpi, which can be blocked with BLT-1, an inhibitor of SR-B1.



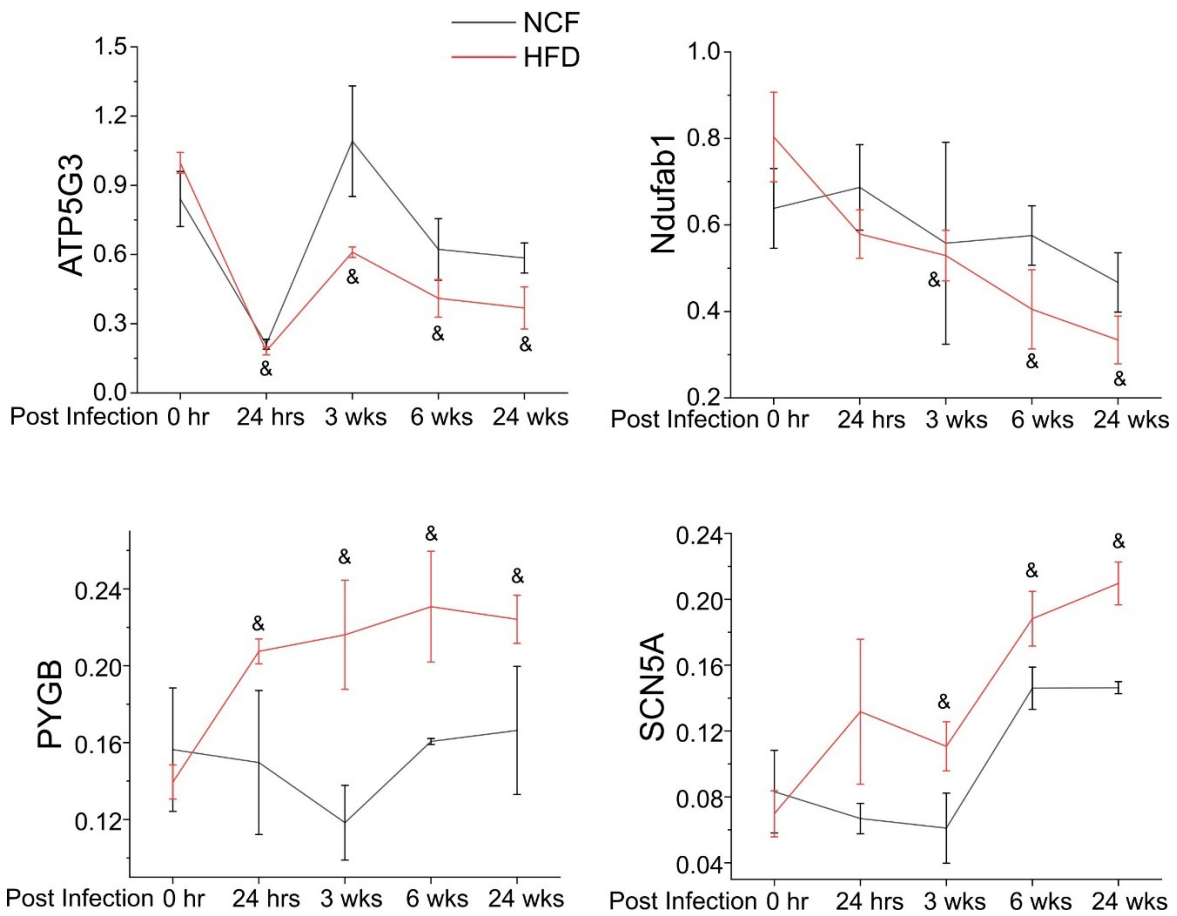
Supplementary Fig 2 (A) The relative protein levels of SR-B1 in kidney, liver, spleen, and lungs in HFD mice and the NCF group by Western blot. Blots from two animals per group were shown. SR-B1 shows two bands in the blots, 75Kd (**) and 84Kd (*), probably due to the distinct post-translational modifications. (B) Relative protein levels of SR-B1 with the 84Kd MW band in hearts and adipose tissues. (C) Relative protein levels of SR-B1 in kidney, liver, spleen, and lungs. (D) Relative ratios of SR-B1 75Kd / 84 Kd MW bands among various tissues. # indicates $p < 0.01$ in HFD vs NCF group for SR-B1. The data from aorta is absent due to the very limited tissue collected.



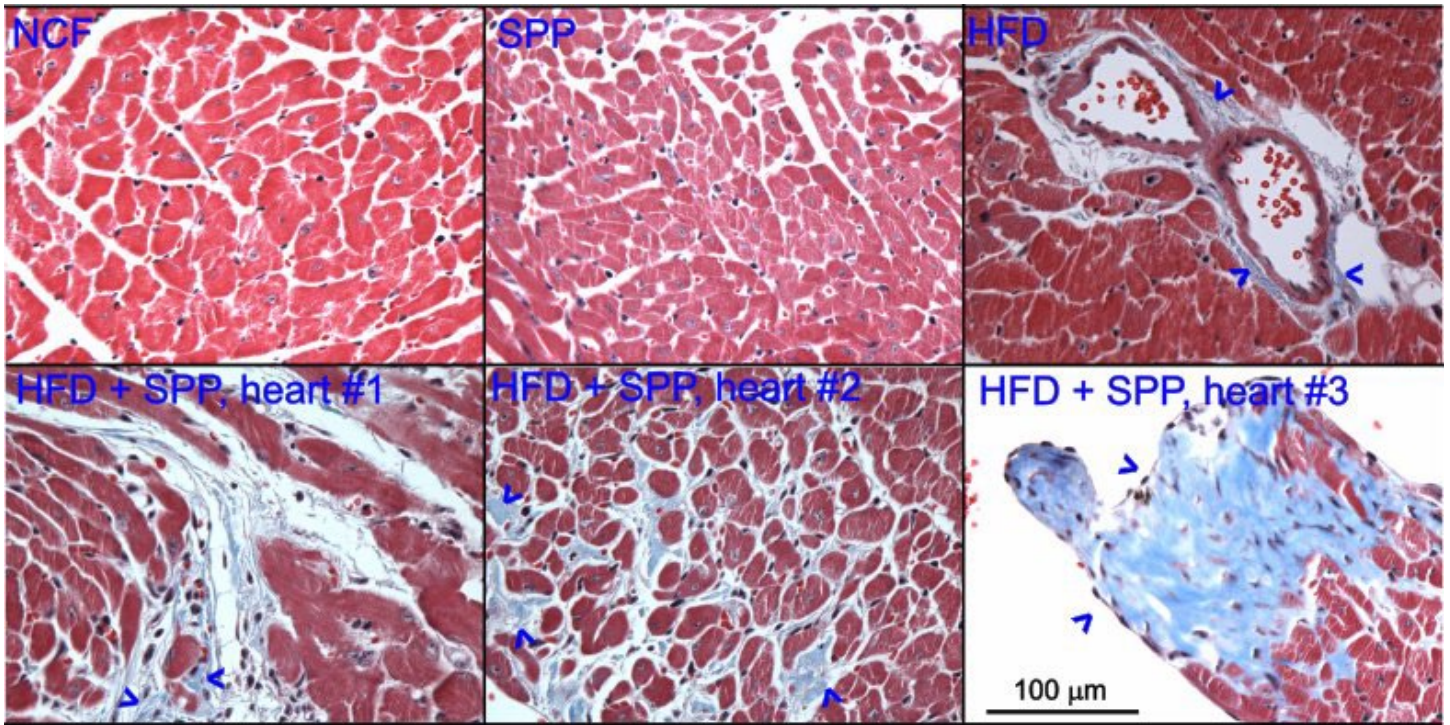
Supplementary Fig 3 Acute changes in cardiac transcriptomes in normal and obese mice 24 hpi. (A) Volcano plot showing the cardiac DEs in NCF mice 24 hpi as compared with control NCF mice without viral administration. (B) Volcano plot showing the cardiac DEs of 24 hpi in HFD mice as compared with NCF mice. (C) Volcano plot showing the cardiac DEs in HFD mice 24 hpi as compared with HFD control mice. (D) Ranked heatmap showing the individual downregulated (left panel) and upregulated DEs (right panel), which is ranked by FDR in HFD mice 24 hpi as compared with HFD control mice. FDR < 0.05 (horizontal dashed line) is used for cut-off threshold. Right vertical dashed line: fold changes (FC) > 0.5 (increase); left vertical dashed line: FC < - 0.5 (decrease). Blue dots represent downregulated DEs and red dots represent upregulated DEs.



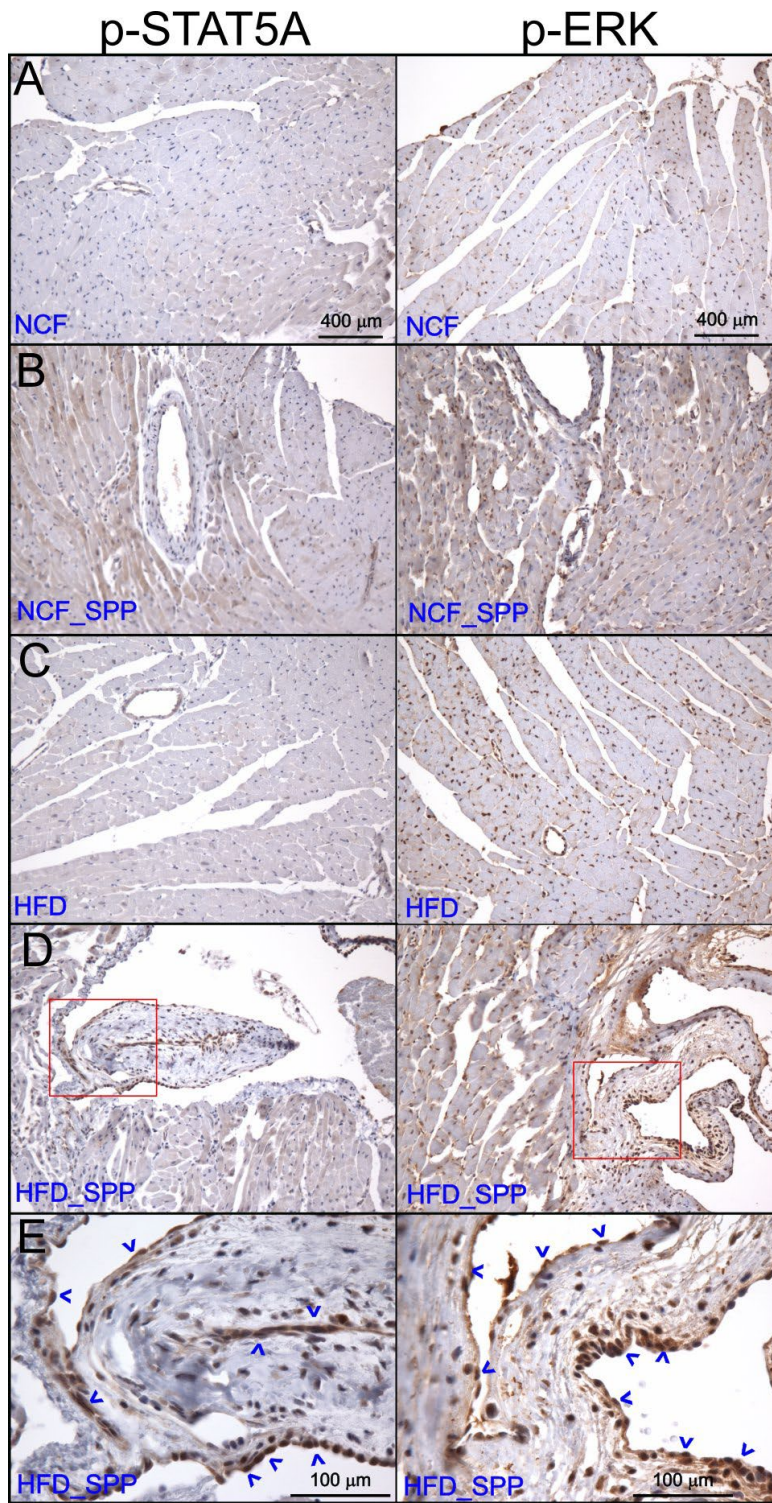
Supplementary Fig 4 (A) Ranked heatmap showing the individual dysregulated DEs, which is ranked by FDR in NCF mice 24 hpi as compared with NCF control mice. (B) Ranked heatmap showing the individual dysregulated DEs, which is ranked by FDR in HFD mice 24 hpi as compared with NCF mice 24 hpi. (C) Volcano plot showing that there is no significant cardiac DEs in NCF mice 3 wpi as compared with control NCF mice without viral administration.



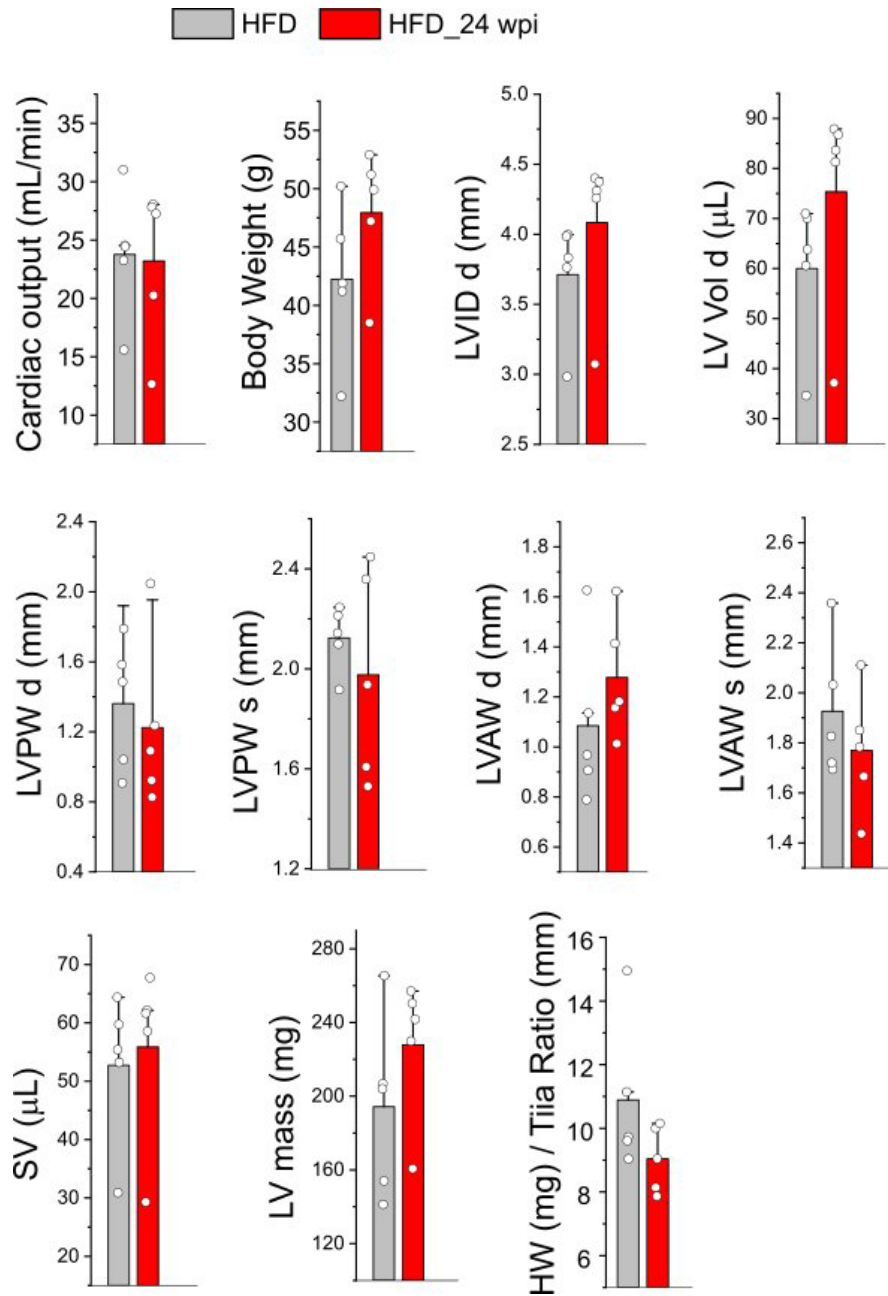
Supplementary Fig 5 Relative changes of some representative cardiac transcripts of DEs in HFD mice during the time course of post viral administration. & indicates $p < 0.05$ at each post-administration time point as compared to before administration (0 hr) in HFD mice.



Supplementary Fig 6 Heart cross section showing the cardiac fibrosis using Masson's trichrome staining. Focal fibrosis was evident in all three examined hearts in the HFD+SPP group but not in the control groups (6 wpi).



Supplementary Fig 7 IHC staining on heart sections (6 wpi) using p-STAT5A and p-ERK antibodies. The boxed areas in (D) were shown in a higher magnification in (E). The arrow heads indicate the positive cells in the focal fibrotic regions.



Supplementary Fig 8 Echocardiogram showing the cardiac functions in the HFD mice 24 wpi as compared with the age-matched HFD controls (13 months old). There were no significant in cardiac output (mL/min), body weight (g) left ventricular end-diastolic diameter (LVID d), left ventricular end-diastolic volume (LV Vol d), left ventricular end-diastolic posterior wall thickness (LVPW d), left ventricular end-systolic posterior wall thickness (LVPW s), left ventricular end-diastolic anterior wall thickness (LVAW d), left ventricular end-systolic anterior wall thickness (LVAW s), and stroke volume (SV), LV mass, and heart weight-to-tibia length.

Supplementary table 1 Source of antibodies in this study

Antibodies	Catalog	Vendor	Dilutions for WB or IHC
Spike S1 subunit	GTX635671	Genetex	1:100 (IHC)
MRC1	A02285-2	Boster Bio	1:200 (IHC)
SR-B1	NB400-104	Novus Biologicals	1:2000
CD31	ZRB1216	Sigma	1:200 (IHC)
STAT5	A21228	Abclonal	1:1000
GAPDH	G8795	Sigma	1:2000
Beta-actin	A1978	Sigma	1:2000
Beta-tubulin	MA1-118	Thermofisher	1:2000
PYGB	A13539	Abclonal	1:1000
OGDH	A6391	Abclonal	1:1000
NDUFS3	A8013	Abclonal	1:1000
NDUFA2	A8136	Abclonal	1:1000
ATP5C1	A15257	Abclonal	1:1000
p-STAT5A	AP0758	Abclonal	1:200 (IHC)
p-ERK	sc-7383	Santa Cruz Biotech	1:200 (IHC)

Supplementary table 2 List of primers

species	ENSEMBL	SYMBOL	ENTREZID	5 primers	3 primers	size
mouse	ENSMUSG00000038717	Atp5l	27425	TAGCCAACAATGCCACGTTT	TTACAGTTAAGGAAGCTGTG	100
mouse	ENSMUSG00000018770	Atp5g3	228033	CTCTCCAGTCCTAGTCTCTG	GGAGAGAGGAAGCGGGAGA	188
mouse	ENSMUSG00000014294	Ndufa2	17991	TTCAGGCTTTGCCGCTTAGC	TGCTTTTGGCCAAGAGAAGA	93
mouse	ENSMUSG00000030869	Ndufab1	70316	CAAGACATACAGAACTCGGT	GCTCGCGCAGGTGCCTGGA	103
mouse	ENSMUSG00000038615	Nfe2l1	18023	AAGCTCTCCCCAGTCTCTCC	CATCGCCAGAAGGAGCAGG	131
mouse	ENSMUSG00000032511	Scn5a	20271	ACTTTCACCTTGGTCCAGTAC	CCGAAGGGGACCTGCCTCT	100
mouse	ENSMUSG00000033059	Pygb	110078	AAGGAGAGTGCCTGTGCATAG	GAGGGGTTCTCTGCCCA	102
mouse	ENSMUSG00000020893	Per1	18626	ATTAGTCAGCCCTCAGAGACA	CGAAACAGGGGAAGGTGAAGA	98
mouse	ENSMUSG00000020456	Ogdh	18293	GACATTTTCACAAAACAAACCAGC	TGGGATTCTCCAACCAGGC	146

Supplementary table 3 Cardiac DEs for NCF_Spp_24hrs vs NCF_CTL

Ensembl ID	Gene symbol	NCF_Spp_24hrs-1	NCF_Spp_24hrs-2	NCF_Spp_24hrs-3	NCF-CTL-1	NCF-CTL-2	NCF-CTL-3	logFC	logCPM	PValue	FDR
ENSG00000121898	CPXM2	8.421097163	4.817468434	5.424727771	61.68102601	53.21796724	49.97904554	-3.13309	4.983498	4.00E-29	4.55E-25
ENSG00000168209	DDIT4	29.00600134	17.34288636	30.57573835	3.304340679	3.130468661	3.010785876	2.992887	3.944127	4.77E-15	2.72E-11
ENSG00000102760	RGCC	37.4270985	27.45957007	27.61679593	8.44442618	8.34791643	6.623728927	1.958697	4.347837	1.60E-11	6.09E-08
ENSG00000136872	ALDOB	4.678387313	0.481746843	2.958942421	26.43472543	30.26119706	12.64530068	-3.07241	3.814489	5.89E-11	1.68E-07
ENSG00000106633	GCK	20.11706544	9.634936868	15.78102624	60.94672808	52.17447769	39.14021639	-1.74582	5.093367	5.53E-10	1.26E-06
ENSG00000104888	SLC17A7	3.74270985	6.744455808	8.876827262	25.33327854	43.30481648	21.67765831	-2.21594	4.259694	2.05E-09	3.89E-06
ENSG00000130037	KCNA5	27.60248514	34.68577273	28.109953	9.913022037	12.00012987	7.225886103	1.613798	4.388355	6.01E-09	9.79E-06
ENSG00000115380	EFEMP1	6.081903506	3.372227904	4.931570701	19.82604407	16.69583286	16.86040091	-1.88824	3.622241	1.37E-08	1.96E-05
ENSG00000161267	BDH1	72.98284208	53.95564646	32.05520956	167.7870767	121.0447882	152.9479225	-1.47294	6.660341	2.47E-08	3.12E-05
ENSG00000118515	SGK1	112.2812955	83.82395075	77.42566001	34.14485368	42.7830717	40.94668791	1.221889	6.049223	4.43E-08	5.05E-05
ENSG00000109854	HTATIP2	4.210548581	7.707949495	8.383670192	24.59898061	28.17421795	17.46255808	-1.7966	4.01015	5.34E-08	5.53E-05
ENSG00000163884	KLF15	54.73713156	47.6929375	60.16516255	18.35744822	24.52200451	27.69923006	1.22443	5.312901	2.12E-07	0.000201
ENSG00000143318	CASQ1	29.00600134	24.56908901	14.7947121	9.545873073	4.695702992	4.817257402	1.77733	3.972161	7.83E-07	0.000644
ENSG00000112992	NNT	404.6805025	396.4776521	625.3231649	256.6371261	209.2196555	142.7112505	1.225113	8.410991	7.92E-07	0.000644
ENSG00000138623	SEMA7A	65.49742238	68.88979861	54.74043478	32.67625783	26.08723884	33.72080181	1.0298	5.583611	2.12E-06	0.001608
ENSG00000173641	HSPB7	431.8151489	346.8577273	398.4709126	678.4912861	742.9645622	624.4369907	-0.79747	9.07175	4.44E-06	0.003159
ENSG00000170989	S1PR1	62.22255126	47.6929375	61.64463376	34.14485368	20.3480463	25.29060136	1.083737	5.426704	6.44E-06	0.004316
ENSG00000176907	C8orf4	43.50900201	36.6127601	34.52099491	23.13038475	13.04361942	13.24745785	1.173706	4.833394	8.86E-06	0.00561
ENSG00000171552	BCL2L1	14.9708394	13.97065846	30.08258128	6.975830323	4.173958215	6.021571752	1.748689	3.773847	9.69E-06	0.005811
ENSG00000157514	TSC22D3	258.2469797	137.2978504	182.4681159	86.64715559	88.17486729	107.1839772	1.038157	7.173171	1.28E-05	0.007267
ENSG00000142733	MAP3K6	14.50300067	8.189696338	29.09626714	4.772936537	3.652213438	3.612943051	2.065179	3.537283	1.45E-05	0.007881
ENSG00000198355	PIM3	56.60848648	36.6127601	62.6309479	27.90332129	25.04374929	13.84961503	1.197181	5.257605	2.31E-05	0.01198
ENSG00000120129	DUSP1	94.03558498	58.29136805	95.17931453	40.38638608	49.04400902	28.30138724	1.064609	5.953111	3.14E-05	0.015572
ENSG00000169764	UGP2	391.5810181	336.2592967	343.2373208	621.9503456	518.6143082	585.8989315	-0.689	8.868002	5.63E-05	0.025688
ENSG00000006283	CACNA1G	38.36277596	46.72944381	51.28833529	22.02893786	27.1307284	22.27981548	0.933805	5.153478	5.64E-05	0.025688
ENSG00000118680	MYL12B	282.1067549	290.0115997	290.4695143	489.7767184	426.7872275	435.3596377	-0.6491	8.531725	8.53E-05	0.036289
ENSG00000100968	NFATC4	3.274871119	4.335721591	2.958942421	8.811575144	11.47838509	10.83882915	-1.52216	2.969313	8.60E-05	0.036289
ENSG00000197217	ENTPD4	32.28087246	22.64210164	36.00046612	70.85975012	57.39192545	46.96825967	-0.95579	5.508345	0.000101	0.040953
ENSG00000136826	KLF4	46.78387313	53.47389962	60.16516255	26.06757647	34.43515527	28.30138724	0.858013	5.408414	0.000117	0.045944
ENSG00000115756	HPCAL1	18.71354925	20.23336742	27.61679593	13.21736272	8.34791643	6.623728927	1.182163	4.077938	0.000121	0.04603

ENSG00000147684	NDUFB9	314.2104676	239.0929155	284.9308333	369.6890633	377.7969971	395.8692702	-0.446174	8.37296	0.00152	0.04243
ENSG00000169122	FAM110B	12.12087857	9.108301545	8.10778794	3.396093758	5.973075053	2.550704061	1.299298	2.98038	0.00152	0.04243
ENSG00000130957	FBP2	13.98562912	11.95464578	15.63644817	8.247656269	4.479806289	7.652112182	1.020713	3.49406	0.00152	0.04243
ENSG00000238193	RP11-555H23.:	601.8482399	580.6542235	589.5520088	300.3117194	294.1739463	532.0768671	0.65378	8.9185	0.00154	0.04301
ENSG00000121691	CAT	139.3901036	148.5791689	229.9137009	101.8828127	68.6903631	133.6568928	0.765927	7.10423	0.00155	0.04314
ENSG00000099901	RANBP1	16.31656731	15.9395277	14.47819275	26.68359381	27.87435025	22.95633655	-0.724822	4.45056	0.00157	0.04347
ENSG00000178996	SNX18	13.98562912	22.77075386	16.21557588	7.762500018	10.45288134	8.672393807	0.963164	3.82331	0.00161	0.04439
ENSG00000159314	ARHGAP27	4.661876374	7.969763851	5.21214939	10.67343752	12.44390636	14.79408355	-1.092904	3.37382	0.00161	0.04447
ENSG00000231500	RPS18	292.7658363	245.3548729	324.8906453	408.9867197	356.8912344	428.5182822	-0.468633	8.42662	0.00162	0.04447
ENSG00000184216	IRAK1	7.925189836	9.677570391	12.74080962	4.851562511	2.488781272	5.101408121	1.258654	3.00285	0.00169	0.04624
ENSG00000082146	STRADB	49.8820772	31.87905541	45.17196138	25.22812506	24.39005646	29.07802629	0.695853	5.14036	0.00169	0.04624
ENSG00000074964	ARHGEF10L	72.2590838	63.18884197	67.75794207	42.6937501	34.84293781	56.11548934	0.607172	5.83446	0.00171	0.04653
ENSG00000092439	TRPM7	59.20582995	69.45079928	62.54579268	82.96171894	100.5467634	88.76450131	-0.512015	6.2921	0.00171	0.04653
ENSG00000174804	FZD4	10.25612802	19.92440963	9.84517107	25.71328131	22.8967877	24.9968998	-0.888379	4.32437	0.00172	0.04653
ENSG00000238181	AHCYP2	2.797125825	4.554150772	4.63302168	1.455468753	0.497756254	0.510140812	2.158903	1.74607	0.00172	0.04653
ENSG00000237541	HLA-DQA2	5.128064012	7.969763851	5.21214939	0	2.488781272	2.550704061	1.82849	2.26897	0.00176	0.04754
ENSG00000146535	GNA12	48.94970193	68.88153043	53.85887703	36.38671883	31.35864403	42.85182822	0.629831	5.57994	0.00176	0.04754
ENSG00000166317	SYNPO2L	47.55113902	48.38785196	53.27974932	35.90156258	29.36761901	34.68957523	0.574481	5.40629	0.00177	0.04754
ENSG00000125148	MT2A	0.466187637	1.138537693	6.37040481	28.13906256	2.488781272	14.79408355	-2.518458	3.33248	0.00179	0.04798
ENSG00000156298	TSPAN7	44.28782556	33.58686195	37.06417344	53.85234387	54.25543173	64.78788314	-0.579605	5.62019	0.0018	0.04822
ENSG00000158125	XDH	37.29501099	34.72539964	35.32679031	65.4960939	35.83845032	97.43689512	-0.885829	5.70648	0.0018	0.04822
ENSG00000244734	HBB	193.4678695	401.9038057	854.7925	196.4882817	237.4297333	228.5430838	1.129364	8.45936	0.00181	0.04828
ENSG00000065978	YBX1	972.001224	879.5203679	871.0080758	1104.700784	1227.466923	1194.749782	-0.373003	10.0262	0.00183	0.04873
ENSG00000107954	NEURL1	3.263313462	2.846344233	4.05389397	0.485156251	0.497756254	1.020281624	2.241317	1.58827	0.00184	0.04882
ENSG00000204628	RACK1	643.3389396	578.9464169	644.5691412	788.378908	782.4728319	846.8337482	-0.372696	9.48233	0.00186	0.04914
ENSG00000088682	COQ9	324.000408	302.2817575	272.1900237	230.9343755	203.582308	234.1546328	0.427234	8.03432	0.00186	0.04914
ENSG00000076555	ACACB	180.4146157	277.8031971	255.9744478	162.0421879	128.9188699	183.6506924	0.58748	7.63466	0.00187	0.04921
ENSG00000196834	POTEI	59.20582995	38.14101272	60.80840955	39.29765634	31.35864403	26.52732223	0.702694	5.44407	0.00187	0.04929
ENSG00000103381	CPPED1	4.195688737	5.123419619	6.94953252	0.485156251	2.986537526	0.510140812	1.964836	2.10541	0.00191	0.04998
ENSG00000100307	CBX7	14.45181676	9.677570391	13.31993733	4.851562511	6.470831307	7.14197137	1.026294	3.36526	0.00191	0.04998
ENSG00000186260	MKL2	20.04606841	11.95464578	17.3738313	31.53515632	32.85191279	21.93605492	-0.793411	4.57587	0.00191	0.04998

ENSG00000146677	AC004453.8	216.328958	133.3521521	190.3250995	231.234207	261.5353334	306.8003	-0.56347	7.809407	0.00214	0.04614
ENSG00000126432	PRDX5	188.3711902	145.6788217	147.5874274	236.4146068	211.8113317	211.7503	-0.45207	7.580959	0.00215	0.04625
ENSG00000170791	CHCHD7	15.1246941	12.88697269	19.37441132	22.1344353	32.93407902	26.93083	-0.77703	4.485252	0.00216	0.04636
ENSG00000120333	MRPS14	28.87441601	28.01515801	32.48063075	41.91414343	51.66130042	42.24444	-0.59609	5.263194	0.00217	0.04651
ENSG00000049283	EPN3	12.37474972	10.08545688	11.39671254	5.18039975	5.811896297	5.808611	1.016922	3.25609	0.00218	0.04666
ENSG00000100644	HIF1A	37.12424916	36.41970542	41.02816516	53.2168338	57.47319671	54.91778	-0.52966	5.574337	0.00221	0.04709
ENSG00000157184	CPT2	60.04045234	58.27152866	55.27405584	30.61145307	43.91210536	42.7725	0.578669	5.629583	0.00221	0.04709
ENSG00000254502	FNTAL1	17.41631442	14.00757901	14.24589068	9.889854069	7.103428807	6.864722	0.921887	3.676712	0.00222	0.0471
ENSG00000204899	MZT1	10.54145346	10.08545688	8.547534408	4.238508887	5.166130042	4.224444	1.109273	3.04099	0.00222	0.0471
ENSG00000171992	SYNPO	42.62413792	39.78152438	68.95011089	34.37901652	20.66452017	32.21139	0.774835	5.355175	0.00222	0.0471
ENSG00000122679	RAMP3	2.749944382	2.801515801	3.98884939	0	1.29153251	0.528056	2.405516	1.549346	0.00223	0.04718
ENSG00000197358	BNIP3P1	43.08246198	57.15092234	63.82159025	26.84388961	46.49517038	22.70639	0.784877	5.462181	0.00224	0.04718
ENSG00000196154	S100A4	11.91642565	8.404547404	11.96654817	17.42498098	20.01875391	20.06611	-0.81516	3.997487	0.00225	0.04732
ENSG00000112972	HMGCS1	23.83285131	39.78152438	27.92194573	17.89592641	20.66452017	13.20139	0.821212	4.633917	0.00227	0.04777
ENSG00000116750	UCHL5	25.2078235	17.92970113	21.08391821	32.4952348	33.57984527	35.90778	-0.65355	4.846604	0.00229	0.04809
ENSG00000234152	ELOBP1	3.208268446	4.482425282	2.849178136	8.006072341	10.33226008	7.392777	-1.26011	2.811037	0.00231	0.04829
ENSG00000131828	PDHA1	395.0753429	446.0013155	352.7282532	297.6375129	323.5288939	266.14	0.429188	8.442572	0.00232	0.04859
ENSG00000168334	XIRP1	27.04111976	67.79668239	43.30750767	31.0823985	12.9153251	23.23444	1.013546	5.142104	0.00234	0.04888
ENSG00000196735	HLA-DQA1	19.70793474	19.61061061	15.95539756	32.02428937	27.76794897	28.515	-0.67471	4.645685	0.00234	0.04881
ENSG00000248746	ACTN3	25.66614756	28.57546117	27.92194573	16.48309011	20.01875391	13.20139	0.733267	4.522845	0.00235	0.04888
ENSG00000188612	SUMO2	176.9130886	172.5733734	120.2353173	185.5525001	248.6200083	257.163	-0.55358	7.602867	0.00236	0.04896
ENSG00000106299	WASL	21.99955505	21.85182325	33.05046638	44.73981602	39.39174157	37.49194	-0.67249	5.091107	0.00237	0.04903
ENSG00000111196	MAGOHB	10.0831294	5.603031602	5.698356272	13.65741752	21.31028642	11.61722	-1.06851	3.616405	0.00239	0.04946
ENSG00000141562	NARF	11.45810159	15.68848849	8.547534408	3.296618023	8.394961318	3.696389	1.259524	3.248421	0.0024	0.04951
ENSG00000108829	LRRCS9	16.49966629	15.12818533	21.08391821	9.418908637	12.26955885	5.280555	0.979562	3.836825	0.00243	0.04998

ENSG00000213619	NDUF53	506.9295589	475.5288907	471.0438823	662.3854829	641.648576	667.328931	-0.43985658	9.159050649	0.000538	0.037803
ENSG00000216938	RPL7P58	3.011462726	1.796143119	5.159297725	12.22286909	7.63867352	8.37432384	-1.52970093	2.873285988	0.000539	0.037803
ENSG00000125730	C3	22.58597045	24.24793211	19.60533136	15.04353119	10.8214542	7.8509286	0.9635675	4.164919699	0.000552	0.038261
ENSG00000107262	BAG1	59.72734407	59.7217587	58.81599407	91.20140786	81.4791842	91.594167	-0.570351	6.222491058	0.000552	0.038261
ENSG00000175920	DOK7	8.532477724	13.02203761	10.83452522	3.290772449	5.09244901	4.71055716	1.32547065	3.123184757	0.000571	0.039117
ENSG00000218175	AC016739.2	142.0406586	197.1267073	171.8046143	238.8160577	241.891328	271.642129	-0.55690822	7.723983145	0.000575	0.039117
ENSG00000117707	PROX1	76.79229951	61.9669376	59.33192384	93.08184926	98.6661996	106.772629	-0.59119145	6.385000058	0.000575	0.039117
ENSG00000197879	MYO1C	84.82286678	105.5234082	95.96293769	64.87522827	57.9266075	67.5179859	0.58658373	6.334999884	0.000582	0.039376
ENSG00000189186	DCAF8L2	9.536298632	10.77685871	4.12743818	1.880441399	2.54622451	2.6169762	1.79364923	2.68224042	0.000589	0.039388
ENSG00000205981	DNAJC19	73.78083679	69.60054586	66.03901089	92.61173891	103.758649	116.193743	-0.57573334	6.45609217	0.000592	0.039388
ENSG00000204564	C6orf136	24.09170181	22.90082477	24.76462908	36.19849693	34.3740308	54.9565002	-0.81012027	5.077646108	0.000593	0.039388
ENSG00000117643	MAN1C1	19.07259726	17.96143119	21.66905045	13.16308979	6.36556127	9.42111432	0.9772114	3.986244112	0.000612	0.04026
ENSG00000215464	AP000354.2	16.56304499	22.00275321	13.93010386	27.73651064	35.6471431	30.8803191	-0.82408064	4.659069341	0.000621	0.04026
ENSG00000179988	PSTK	8.030567269	7.184572476	8.770806133	15.98375189	14.0042348	17.7954382	-1.00188922	3.687611638	0.000622	0.04026
ENSG00000075415	SLC25A3	2527.621048	2417.608638	2598.738264	3280.900131	3509.33393	3301.57717	-0.41974265	11.521633	0.000625	0.04026
ENSG00000185088	RPS27L	3.011462726	7.633608255	8.254876361	11.75275874	14.6407909	19.3656239	-1.25867786	3.540222934	0.000625	0.04026
ENSG00000172586	CHCHD1	31.11844817	36.82093394	27.34427795	52.65235918	44.5589289	56.5266859	-0.68947006	5.408636354	0.000627	0.04026
ENSG00000070087	PFN2	72.77701588	63.76308072	62.94343225	96.84273206	108.851098	91.0707717	-0.57001583	6.382966584	0.000635	0.040527
ENSG00000219470	RP3-337H4.6	128.4890763	162.5509523	108.861182	208.7289953	187.147501	206.217724	-0.58888104	7.391950521	0.000641	0.04067
ENSG00000108262	GIT1	64.74644861	74.09090365	61.39564293	44.66048323	40.7395921	45.0119906	0.6167973	5.817058334	0.000654	0.041031
ENSG00000159592	GPBP1L1	51.69677768	35.4738266	61.91157271	76.15787667	77.6598474	88.4537955	-0.70576038	6.043648306	0.000656	0.041031
ENSG00000204396	VWA7	8.030567269	8.082644035	11.350455	4.701103498	1.90966838	3.14037144	1.41907234	2.879189326	0.000657	0.041031
ENSG00000254112	KB-1205A7.1	40.15283635	38.61707706	40.75845203	47.48114533	68.7480617	85.8368193	-0.75315283	5.762440475	0.00067	0.041565
ENSG00000149428	HYOU1	37.14137362	43.55647063	39.21066271	28.20662099	20.369796	23.5527858	0.72040604	5.057357629	0.000673	0.041565
ENSG00000182446	NPOC4	38.64710498	30.9834688	59.33192384	27.26640029	21.0063522	19.3656239	0.91716635	5.08446979	0.000686	0.042115
ENSG00000139112	GABARAPL1	60.73116498	66.4572954	71.71423838	41.83982113	41.3761482	46.5821763	0.61354409	5.806823229	0.00069	0.042115
ENSG00000168273	SMIM4	41.15665726	53.88429357	34.05136499	59.70401442	75.7501791	74.8455193	-0.69341236	5.841643152	0.000724	0.043951
ENSG00000105953	OGDH	1653.794947	1258.198255	1815.55687	1209.59393	863.170108	1041.55653	0.60140969	10.35346778	0.000752	0.045416
ENSG00000137692	DCUN1D5	81.81140406	73.19283209	79.45318497	104.3644977	121.58222	114.623558	-0.53646259	6.593624491	0.000756	0.045416
ENSG00000134531	EMP1	16.06113454	22.45178899	18.05754204	39.95937973	29.9181379	29.3101334	-0.81067416	4.75237932	0.000764	0.045652
ENSG00000163382	NAXE	53.20250816	43.10743485	55.20448566	78.03831807	77.0232913	73.2753336	-0.59486411	6.002594267	0.000778	0.046291
ENSG00000075886	TUBA3D	1.505731363	8.082644035	4.12743818	9.402206996	14.0042348	15.178462	-1.44422322	3.259256868	0.000787	0.046566
ENSG00000180957	PITPNB	31.62035862	35.4738266	39.72659249	19.74463469	22.2794644	22.5059953	0.72943383	4.892287901	0.000796	0.046807
ENSG00000082641	NFE2L1	750.3561292	738.2148219	758.4167656	561.781868	543.618932	575.734764	0.41819655	9.357307316	0.000799	0.046807
ENSG00000143393	PI4KB	52.70059771	46.25068531	57.78413453	33.37783484	38.1933676	23.0293906	0.7326639	5.425524463	0.000809	0.047152
ENSG00000141562	NARF	10.03820909	11.67493027	16.50975272	3.290772449	8.27522965	3.66376668	1.36823765	3.313212792	0.000824	0.047539
ENSG00000197852	FAM212B	5.019104543	7.184572476	8.254876361	2.350551749	1.90966838	2.09358096	1.64472908	2.482246996	0.000824	0.047539
ENSG00000163735	CXCL5	4.517194089	4.041322018	3.611508408	6.581544897	14.0042348	11.5146953	-1.35631957	3.027057639	0.000839	0.048154
ENSG00000185834	RPL12P4	11.04203	20.65564587	11.86638477	27.73651064	28.6450257	25.6463667	-0.89413473	4.448623019	0.000846	0.048304
ENSG00000087302	C14orf166	127.9871659	126.1790541	120.211637	173.9408294	169.32393	178.477777	-0.47891567	7.231035144	0.000856	0.048485
ENSG00000165629	ATP5C1	695.1459793	636.2836999	673.8042829	886.6281197	1043.95205	841.09615	-0.46646015	9.63811376	0.000858	0.048485
ENSG00000230807	AC099535.4	3.51337318	2.245178899	3.611508408	7.991875946	7.00211739	9.94450956	-1.41888377	2.734025581	0.000877	0.049319
ENSG00000121898	CPXM2	36.63946317	36.82093394	35.08322453	17.39408294	23.5525767	24.5995763	0.7377722	4.913529666	0.000883	0.049411
ENSG00000204220	PFDN6	13.55158227	19.30853853	11.350455	30.08706239	30.5546941	21.9826001	-0.88566101	4.460860419	0.000897	0.049941
ENSG00000159388	BTG2	19.57450772	18.85950275	12.89824431	8.461986296	9.5483419	7.32753336	1.02674819	3.801256386	0.000905	0.049948
ENSG00000142733	MAP3K6	6.022925452	11.22589449	11.86638477	1.880441399	3.18278063	5.2339524	1.49852777	2.944952804	0.000913	0.049948
ENSG00000175390	EIF3F	24.59361226	30.53443302	26.82834817	44.66048323	42.0127044	42.9184097	-0.65814678	5.176790818	0.000914	0.049948
ENSG00000170035	UBE2E3	109.9183895	89.80715594	100.6063056	148.5548705	135.586455	144.980481	-0.51764844	6.936010385	0.000918	0.049948
ENSG00000150527	CTAGE5	18.57068681	20.65564587	22.18498022	31.96750379	35.6471431	33.4972953	-0.71359477	4.802861986	0.000919	0.049948

Supplementary Table 7 Prediction of Stat5-regulated targeted genes in this study from the existing Cistromes data [46-49]

Target gene	Biosamples	MASC2 binding score	MASC2 Q value	DOI (Signaling Pathways Project Datasets)*	Ref
ATP5C1	B lymphocytes, GM12878 cells	185	1< E-05	10.1621/WdnDiLYKWM	[46]
ATP5G3	Fibroblasts, MEFs	142	1< E-05	10.1621/xXhMIGXpPo	[47]
	Mammary gland	159	1< E-05	10.1621/w9eiy79IrX	[48]
	myeloblasts, K562 cells	176	1< E-05	10.1621/WdnDiLYKWM	[46]
ATP5L	Mammary gland	85, 92	1< E-05	10.1621/w9eiy79IrX	[48]
ATP5MK (USMG5)	B lymphocytes, GM12878 cells	162	1< E-05	10.1621/WdnDiLYKWM	[46]
NDUFA2	B lymphocytes, GM12878 cells	121	1< E-05	10.1621/WdnDiLYKWM	[46]
	myeloblasts, K562 cells	1319	1< E-05	10.1621/WdnDiLYKWM	[46]
	T lymphocytes, CD4+	95, 119	1< E-05	10.1621/ISZJ58eZyg	[49]
	Mammary gland	106, 164, 176,	1< E-05	10.1621/w9eiy79IrX	[48]
NDUFAB1	Fibroblasts, MEFs	374	1< E-05	10.1621/xXhMIGXpPo	[47]
	myeloblasts, K562 cells	139	1< E-05	10.1621/WdnDiLYKWM	[46]
	B lymphocytes, GM12878 cells	174	1< E-05	10.1621/WdnDiLYKWM	[46]
	Fibroblasts, MEFs	145	1< E-05	10.1621/xXhMIGXpPo	[47]
NDUFA1	T lymphocytes, CD4+	77, 108	1< E-05	10.1621/ISZJ58eZyg	[49]
	B lymphocytes, GM12878 cells	73	1< E-05	10.1621/WdnDiLYKWM	[46]
NDUFS3	Mammary gland	111	1< E-05	10.1621/w9eiy79IrX	[48]
PYGB	Mammary gland	158	1< E-05	10.1621/w9eiy79IrX	[48]
OGDH	Fibroblasts, MEFs	101	1< E-05	10.1621/xXhMIGXpPo	[47]
MFN2	Fibroblasts, MEFs	103	1< E-05	10.1621/xXhMIGXpPo	[47]
	Mammary gland	135	1< E-05	10.1621/w9eiy79IrX	[48]
	T lymphocytes, CD4+	149	1< E-05	10.1621/ISZJ58eZyg	[49]
GNA12	B lymphocytes, GM12878 cells	150	1< E-05	10.1621/WdnDiLYKWM	[46]
	myeloblasts, K562 cells	446	1< E-05	10.1621/WdnDiLYKWM	[46]
GYS1	Fibroblasts, MEFs	138	1< E-05	10.1621/xXhMIGXpPo	[47]
SCN5A	Mammary gland	224	1< E-05	10.1621/w9eiy79IrX	[48]
PER1	Mammary gland	102, 208, 252, 277,329,468	1< E-05	10.1621/w9eiy79IrX	[48]
	Fibroblasts, MEFs	98	1< E-05	10.1621/xXhMIGXpPo	[47]
SLC6A6	myeloblasts, K562 cells	121	1< E-05	10.1621/WdnDiLYKWM	[46]
	Fibroblasts, MEFs	93, 316	1< E-05	10.1621/xXhMIGXpPo	[47]

*Signaling Pathways Project Datasets: <http://www.signalingpathways.org/index.jsf>

References

- [1] Cao X, Tian Y, Nguyen V, et al. Spike protein of sars-cov-2 activates macrophages and contributes to induction of acute lung inflammation in male mice. *FASEB J.* 2021;35:e21801.10.1096/fj.202002742RR.
- [2] Kimura T, Mogi C, Tomura H, et al. Induction of scavenger receptor class b type i is critical for simvastatin enhancement of high-density lipoprotein-induced anti-inflammatory actions in endothelial cells. *J Immunol* 2008;181:7332-7340.10.4049/jimmunol.181.10.7332.
- [3] Lee SW, Kim SY, Moon SY, et al. Statin use and covid-19 infectivity and severity in south korea: Two population-based nationwide cohort studies. *JMIR Public Health Surveill* 2021;7:e29379.10.2196/29379.
- [4] Kollias A, Kyriakoulis KG, Kyriakoulis IG, et al. Statin use and mortality in covid-19 patients: Updated systematic review and meta-analysis. *Atherosclerosis* 2021;330:114-121.10.1016/j.atherosclerosis.2021.06.911.
- [5] Surma S, Banach M, Lewek J. Covid-19 and lipids. The role of lipid disorders and statin use in the prognosis of patients with sars-cov-2 infection. *Lipids Health Dis* 2021;20:141.10.1186/s12944-021-01563-0.
- [6] Pawlos A, Niedzielski M, Gorzelak-Pabis P, et al. Covid-19: Direct and indirect mechanisms of statins. *Int J Mol Sci* 2021;22.10.3390/ijms22084177.
- [7] Reiner Z, Hatamipour M, Banach M, et al. Statins and the covid-19 main protease: In silico evidence on direct interaction. *Arch Med Sci* 2020;16:490-496.10.5114/aoms.2020.94655.
- [8] Cariou B, Goronflot T, Rimbart A, et al. Routine use of statins and increased covid-19 related mortality in inpatients with type 2 diabetes: Results from the coronado study. *Diabetes Metab* 2021;47:101202.10.1016/j.diabet.2020.10.001.
- [9] Raman B, Bluemke DA, Luscher TF, et al. Long covid: Post-acute sequelae of covid-19 with a cardiovascular focus. *Eur. Heart J.* 2022;43:1157-1172.10.1093/eurheartj/ehac031.
- [10] Lindner D, Fitzek A, Brauning H, et al. Association of cardiac infection with sars-cov-2 in confirmed covid-19 autopsy cases. *JAMA Cardiol* 2020;5:1281-1285.10.1001/jamacardio.2020.3551.
- [11] Vrints CJM, Krychtiuk KA, Van Craenenbroeck EM, et al. Endothelialitis plays a central role in the pathophysiology of severe covid-19 and its cardiovascular complications. *Acta Cardiol.* 2021;76:109-124.10.1080/00015385.2020.1846921.
- [12] Robinson FA, Mihealsick RP, Wagener BM, et al. Role of angiotensin-converting enzyme 2 and pericytes in cardiac complications of covid-19 infection. *Am J Physiol Heart Circ Physiol* 2020;319:H1059-H1068.10.1152/ajpheart.00681.2020.
- [13] Daems M, Liesenborghs L, Cuijpers I, et al. Sars-cov-2 infection leads to cardiac pericyte loss, fibrosis, cardiomyocyte hypertrophy, and diastolic dysfunction. *Researchsquare.com* 2020.10.21203/rs.3.rs-105963/v1.
- [14] Avolio E, Carrabba M, Milligan R, et al. The sars-cov-2 spike protein disrupts human cardiac pericytes function through cd147 receptor-mediated signalling: A potential non-infective mechanism of covid-19 microvascular disease. *Clin. Sci. (Lond.)* 2021;135:2667-2689.10.1042/CS20210735.
- [15] Guzik TJ, Mohiddin SA, Dimarco A, et al. Covid-19 and the cardiovascular system: Implications for risk assessment, diagnosis, and treatment options. *Cardiovasc. Res.* 2020;116:1666-1687.10.1093/cvr/cvaa106.
- [16] Wang EY, Mao T, Klein J, et al. Diverse functional autoantibodies in patients with covid-19. *Nature* 2021;595:283-288.10.1038/s41586-021-03631-y.
- [17] Cuthbertson DJ, Steele T, Wilding JP, et al. What have human experimental overfeeding studies taught us about adipose tissue expansion and susceptibility to obesity and metabolic complications? *Int J Obes (Lond)* 2017;41:853-865.10.1038/ijo.2017.4.
- [18] Mizunoe Y, Kobayashi M, Tagawa R, et al. Association between lysosomal dysfunction and obesity-related pathology: A key knowledge to prevent metabolic syndrome. *Int J Mol Sci* 2019;20.10.3390/ijms20153688.
- [19] Hamazaki J, Murata S. Er-resident transcription factor nrf1 regulates proteasome expression and beyond. *Int J Mol Sci* 2020;21.10.3390/ijms21103683.
- [20] Yamamoto S, Ogasawara N, Yamamoto K, et al. Mitochondrial proteins nip-snap-1 and -2 are a target for the immunomodulatory activity of clarithromycin, which involves nf-kappab-mediated cytokine production. *Biochem Biophys Res Commun* 2017;483:911-916.10.1016/j.bbrc.2016.12.100.
- [21] McLelland GL, Fon EA. Mfn2 retrotranslocation boosts mitophagy by uncoupling mitochondria from the er. *Autophagy* 2018;14:1658-1660.10.1080/15548627.2018.1505154.
- [22] Yap ZY, Efthymiou S, Seiffert S, et al. Bi-allelic variants in ogdhl cause a neurodevelopmental spectrum disease featuring epilepsy, hearing loss, visual impairment, and ataxia. *Am. J. Hum. Genet.* 2021;108:2368-2384.10.1016/j.ajhg.2021.11.003.

- [23] Mathieu C, Li de la Sierra-Gallay I, Duval R, et al. Insights into brain glycogen metabolism: The structure of human brain glycogen phosphorylase. *J. Biol. Chem.* 2016;291:18072-18083.10.1074/jbc.M116.738898.
- [24] Wende AR, Brahma MK, McGinnis GR, et al. Metabolic origins of heart failure. *JACC Basic Transl Sci* 2017;2:297-310.10.1016/j.jacbts.2016.11.009.
- [25] Tran DH, Wang ZV. Glucose metabolism in cardiac hypertrophy and heart failure. *J Am Heart Assoc* 2019;8:e012673.10.1161/JAHA.119.012673.
- [26] Wilde AAM, Amin AS. Clinical spectrum of scn5a mutations: Long qt syndrome, brugada syndrome, and cardiomyopathy. *JACC Clin Electrophysiol* 2018;4:569-579.10.1016/j.jacep.2018.03.006.
- [27] Ansar M, Ranza E, Shetty M, et al. Taurine treatment of retinal degeneration and cardiomyopathy in a consanguineous family with slc6a6 taurine transporter deficiency. *Hum. Mol. Genet.* 2020;29:618-623.10.1093/hmg/ddz303.
- [28] Lindstrom S, Wang L, Smith EN, et al. Genomic and transcriptomic association studies identify 16 novel susceptibility loci for venous thromboembolism. *Blood* 2019;134:1645-1657.10.1182/blood.2019000435.
- [29] Jesus ICG, Araujo FM, Mesquita T, et al. Molecular basis of period 1 regulation by adrenergic signaling in the heart. *FASEB J.* 2021;35:e21886.10.1096/fj.202100441R.
- [30] Davidson AJ, London B, Block GD, et al. Cardiovascular tissues contain independent circadian clocks. *Clin. Exp. Hypertens.* 2005;27:307-311.
- [31] Leibetseder V, Humpeler S, Svoboda M, et al. Clock genes display rhythmic expression in human hearts. *Chronobiol. Int.* 2009;26:621-636.10.1080/07420520902924939.
- [32] Rykaczewska U, Suur BE, Rohl S, et al. Pcsk6 is a key protease in the control of smooth muscle cell function in vascular remodeling. *Circ. Res.* 2020;126:571-585.10.1161/CIRCRESAHA.119.316063.
- [33] Waudby-West R, Parcell BJ, Palmer CNA, et al. The association between sars-cov-2 rt-pcr cycle threshold and mortality in a community cohort. *Eur. Respir. J.* 2021;58.10.1183/13993003.00360-2021.
- [34] Whitaker M, Elliott J, Chadeau-Hyam M, et al. Persistent covid-19 symptoms in a community study of 606,434 people in england. *Nat Commun* 2022;13:1957.10.1038/s41467-022-29521-z.
- [35] Heubner L, Petrick PL, Guldner A, et al. Extreme obesity is a strong predictor for in-hospital mortality and the prevalence of long-covid in severe covid-19 patients with acute respiratory distress syndrome. *Sci. Rep.* 2022;12:18418.10.1038/s41598-022-22107-1.
- [36] Valenzuela G, Alarcon-Andrade G, Schulze-Schiapacasse C, et al. Short-term complications and post-acute sequelae in hospitalized paediatric patients with covid-19 and obesity: A multicenter cohort study. *Pediatr. Obes.* 2022:e12980.10.1111/ijpo.12980.
- [37] Carfi A, Bernabei R, Landi F, et al. Persistent symptoms in patients after acute covid-19. *JAMA* 2020;324:603-605.10.1001/jama.2020.12603.
- [38] Diez-Fuertes F, Iglesias-Caballero M, Garcia-Perez J, et al. A founder effect led early sars-cov-2 transmission in spain. *J. Virol.* 2021;95.10.1128/JVI.01583-20.
- [39] Fernandez-de-Las-Penas C, Cancela-Celleruelo I, Rodriguez-Jimenez J, et al. Associated-onset symptoms and post-covid-19 symptoms in hospitalized covid-19 survivors infected with wuhan, alpha or delta sars-cov-2 variant. *Pathogens* 2022;11.10.3390/pathogens11070725.
- [40] Spinicci M, Graziani L, Tilli M, et al. Infection with sars-cov-2 variants is associated with different long covid phenotypes. *Viruses* 2022;14.10.3390/v14112367.
- [41] Antonelli M, Pujol JC, Spector TD, et al. Risk of long covid associated with delta versus omicron variants of sars-cov-2. *Lancet* 2022;399:2263-2264.10.1016/S0140-6736(22)00941-2.
- [42] Lopez-Cortes GI, Palacios-Perez M, Velez HF, et al. The spike protein of sars-cov-2 is adapting because of selective pressures. *Vaccines (Basel)* 2022;10.10.3390/vaccines10060864.
- [43] Wang C, Liu B, Zhang S, et al. Differences in incidence and fatality of covid-19 by sars-cov-2 omicron variant versus delta variant in relation to vaccine coverage: A world-wide review. *J. Med. Virol.* 2022.10.1002/jmv.28118.
- [44] Boglione L, Meli G, Poletti F, et al. Risk factors and incidence of long-covid syndrome in hospitalized patients: Does remdesivir have a protective effect? *QJM* 2022;114:865-871.10.1093/qjmed/hcab297.
- [45] Ayoubkhani D, Bermingham C, Pouwels KB, et al. Trajectory of long covid symptoms after covid-19 vaccination: Community based cohort study. *BMJ* 2022;377:e069676.10.1136/bmj-2021-069676.
- [46] Gertz J, Savic D, Varley KE, et al. Distinct properties of cell-type-specific and shared transcription factor binding sites. *Mol Cell* 2013;52:25-36.10.1016/j.molcel.2013.08.037.

- [47] Zhu BM, Kang K, Yu JH, et al. Genome-wide analyses reveal the extent of opportunistic stat5 binding that does not yield transcriptional activation of neighboring genes. *Nucleic Acids Res* 2012;40:4461-4472.10.1093/nar/gks056.
- [48] Shin HY, Willi M, HyunYoo K, et al. Hierarchy within the mammary stat5-driven wap super-enhancer. *Nat Genet* 2016;48:904-911.10.1038/ng.3606.
- [49] Villarino A, Laurence A, Robinson GW, et al. Signal transducer and activator of transcription 5 (stat5) paralog dose governs t cell effector and regulatory functions. *Elife* 2016;5.10.7554/eLife.08384.